Modifying the Mechanical Property of PLA-Carbon Fiber Composite Fabricated by FDM Via Adjusting Process Parameters and Heat Treatment

Yuchao Bai[1], Yihan Xiao[1], Yilin Wang[2], Yilin Liang[1], Yu Yan[1] and Cuiling Zhao[1,*]

[1]*School of Robotics and Advanced Manufacture, Harbin Institute of Technology, Shenzhen, 518055, China*

[2]*School of Materials Science and Engineering, Harbin Institute of Technology, Weihai, 264209, China*

Abstract: Fused deposition modeling (FDM) has become one of the most widely used additive manufacturing technologies, while polylactic acid reinforced by short carbon fibers (PLA-CF) is increasingly applied in structural components. However, the mechanical properties of FDM-printed parts are strongly affected by printing parameters and show obvious anisotropy owing to weak interlayer bonding. In this work, PLA-CF composites with fiber mass fractions of 4 wt.%, 7 wt.%, and 15 wt.% were prepared by FDM. The effects of filling angle (0°, 45°, 90°), printing hatch (0.35 mm, 0.45 mm), and annealing treatment on tensile properties and mechanical anisotropy were systematically studied. The results show that filling angle dominates the tensile strength, which reaches the maximum at 0° filling angle due to favorable fiber alignment and load transfer. Reducing printing hatch can improve interlayer bonding and significantly enhance the strength of 45° and 90° specimens. The fiber mass fraction presents an angle-dependent influence on tensile performance. Moreover, heat treatment effectively reduces anisotropy. Vacuum annealing at 180°C for 3 h increases the tensile strength of 90° specimens by 105.6% and minimizes the strength gap between 0° and 90° specimens to only 2.5 MPa. This work provides a feasible strategy for preparing high-performance, low-anisotropy PLA-CF components.

Keywords: Fused deposition modeling, PLA-carbon fiber, Mechanical property, Process parameters, Heat treatment.

1. INTRODUCTION

Additive manufacturing (AM), widely recognized as a transformative industrial technology, has reshaped the design and production paradigm of advanced components by enabling layer-by-layer fabrication of complex geometries with high material efficiency, short development cycles, and excellent design flexibility [1-3]. Among the seven types of additive manufacturing technologies in ISO/ASTM 52900:2021, fused deposition modeling (FDM) stands out as the most mature and cost-effective technique for polymeric materials, which has been extensively employed in automotive, aerospace, biomedical, and daily consumer products [4-7]. Nevertheless, the layer-by-layer deposition mechanism of FDM often results in interlayer voids, insufficient bonding, and pronounced mechanical anisotropy, which collectively compromise the structural integrity and load-bearing capacity of printed components [8, 9]. Consequently, improving the mechanical performance and structural reliability of FDM-printed polymer composites remains an important research challenge.

Polylactic acid (PLA), a biocompatible polyester derived from renewable resources such as corn starch and sugarcane, has become one of the most popular feedstocks for FDM owing to its low printing temperature, limited warpage and good processability [10-12]. Moreover, compared with petroleum-based polymers such as ABS and PC, PLA can be completely degraded into carbon dioxide and water under specific conditions, which effectively alleviates environmental pollution. However, the intrinsic brittleness, low tensile strength, and insufficient heat resistance of pure PLA severely limit its application in high-performance structural components that bear continuous loads [13]. Incorporating short carbon fibers into PLA has therefore become an effective approach to enhancing its stiffness, specific strength, and thermal performance [14, 15]. However, the mechanical properties of FDM-printed PLA/carbon fiber (PLA-CF) composites are governed not only by the intrinsic properties of the constituents but also by fiber distribution, interfacial load transfer, void formation, and the quality of interlayer bonding. These characteristics are strongly influenced by printing parameters, making the optimization of the processing conditions essential for achieving reliable mechanical performance.

Extensive research has confirmed that the mechanical performance of PLA-CF composites printed by FDM is highly sensitive to multiple processing parameters, such as filling angle, printing temperature, layer thickness, and printing speed [14, 16, 17]. Among these parameters, infill orientation directly affects the alignment of the deposited material relative to the loading direction and, consequently, the

*Address correspondence to this author at the School of Robotics and Advanced Manufacture, Harbin Institute of Technology, Shenzhen, 518055, China; E-mail: zhaocuiling@hit.edu.cn

Received on 06-09-2026 Accepted on 19-10-2026 Published on 22-10-2026

E-ISSN: 2311-8717/26

efficiency of stress transfer. In addition to orientation, carbon fiber content and printing hatch spacing may jointly influence the internal architecture of the deposited composite. Increasing the fiber content can enhance stiffness and load-bearing capacity, whereas excessive fiber loading may promote fiber agglomeration, insufficient matrix impregnation, and interfacial stress concentration. Similarly, hatch spacing affects the overlap and contact between adjacent deposition roads, thereby influencing inter-road bonding and the formation of internal voids. These effects are potentially interdependent: the influence of fiber content on mechanical performance may vary with infill orientation and hatch spacing because these parameters collectively determine the distribution of reinforcing fibers, matrix continuity, and defect evolution. However, the combined effects of these parameters on tensile behavior and fracture mechanisms remain insufficiently understood. In particular, a systematic relationship among processing conditions, internal microstructural characteristics, and tensile failure behavior is needed to clarify how the interaction between fiber reinforcement and deposition architecture governs the mechanical performance of PLA-CF composites.

Furthermore, the layer-by-layer deposition nature of FDM inevitably causes weak interlayer bonding and significant mechanical anisotropy, resulting in noticeable performance differences between parallel and perpendicular printing directions [17]. To address this defect, heat treatment (annealing) has been recognized as an effective post-processing method to promote molecular chain diffusion, eliminate interlayer voids, and thus improve interlayer bonding strength to reduce anisotropy [18, 19]. Meanwhile, annealing can also increase the crystallinity of the PLA matrix and enhance the interfacial bonding ability between PLA and carbon fibers, further improving the overall mechanical properties of the components [20, 21]. During conventional heat treatment in an air environment, the pre-existing interlayer pores in the samples and moisture absorbed within the material evaporate under heat, easily generating new pores in the matrix and reducing the density of the formed components. Under vacuum heat treatment conditions, the pressure difference between the inside and outside can promote the escape of internal pores, effectively increasing the sample density. Nevertheless, the relationship between vacuum-assisted thermal treatment, microstructural evolution, and the mechanical anisotropy of FDM-printed PLA-CF composites has not been sufficiently established. In particular, the extent to which vacuum annealing can improve tensile performance while mitigating orientation-dependent mechanical differences requires further experimental investigation.

To address these knowledge gaps, this study systematically investigates the effects of carbon fiber content, infill orientation, and printing hatch spacing on the tensile properties of FDM-printed PLA-CF composites and further evaluates the potential of vacuum annealing to improve their mechanical performance. Tensile tests are carried out in accordance with the standard GB/T 1447-2005. The fracture micromorphology of specimens is observed via scanning electron microscopy (SEM) to clarify the tensile failure mechanism of the composites. Meanwhile, differential scanning calorimetry (DSC) is employed to determine the optimal annealing temperature of the PLA-CF composites. Heat treatment is performed using a muffle furnace and a vacuum drying oven to optimize the process. By integrating processing-parameter analysis, fracture-surface characterization, thermal analysis, and post-processing evaluation, this study aims to establish a processing–microstructure–property relationship for FDM-printed PLA-CF composites. The findings are expected to provide a basis for optimizing both printing and post-processing strategies to improve the mechanical reliability of short-carbon-fiber-reinforced PLA components.

2. MATERIALS AND METHODS

The overall experimental process is shown in Figure **1**. The experimental materials and methods are described in details below.

2.1. Materials and Specimen Preparation

Three distinct formulations of short carbon fiber-reinforced PLA composites with controlled mass fractions were selected to investigate the correlation between fiber content and mechanical performance. The diameter of filament was 1.75 mm, and the short carbon fiber mass fraction was 4wt.%,7wt.% and 15wt.%, respectively. Tensile specimens were fabricated via a Bambu Lab X1 Carbon FDM 3D printer (Shenzhen Tuozhu Technology Co., Ltd., China) under controlled printing parameters. In accordance with GB/T 1447-2005, the type I dog-bone specimens featuring a 3 mm thickness, 10 mm width, and 50 mm gauge length were designed to print. The specimens were computationally modeled in SolidWorks, exported as STL files, and processed through Bambu Studio slicer software.

2.2. Process and Anneal Parameter

The process parameters of FDM used in this study are detailed in Table **1**. The fiber content of the short carbon fiber-reinforced filament was selected based on common specifications in the consumer market; the filling angles were set to 0°, 45°, and 90°, and the

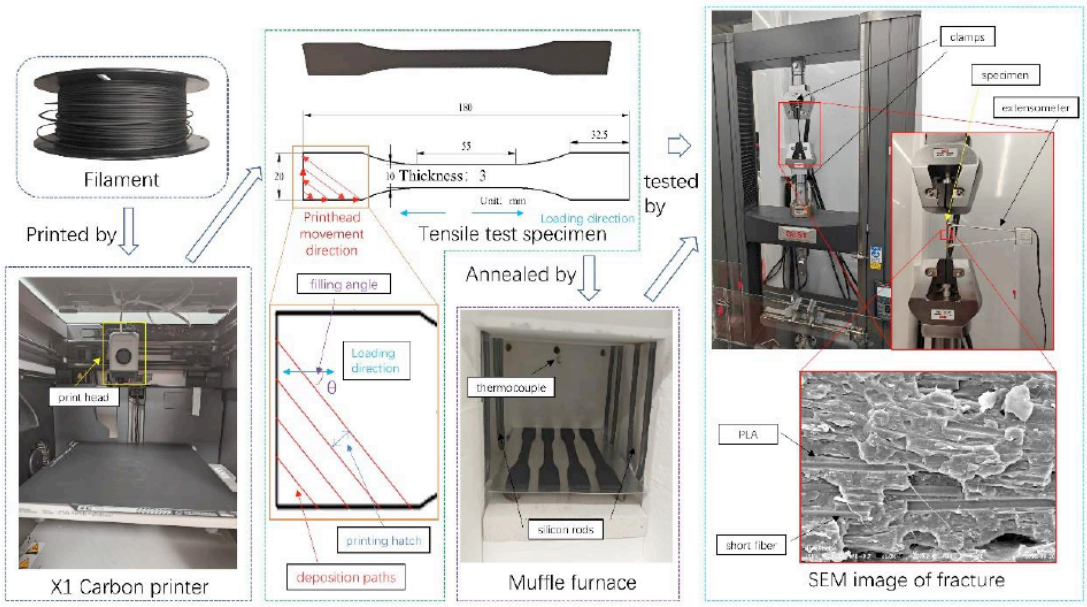


Figure 1: The overall experimental process from additive manufacturing to performance characterization.

printing hatch to 0.35 mm and 0.45 mm—parameters established based on optimized printing processes for the PLA matrix material. During FDM manufacturing, multiple process parameters significantly influence the mechanical properties of the fabricated specimens. This work systematically investigates the effect of short carbon fiber mass fraction on the performance of the composites, with particular focus on the mechanisms by which two key parameters—filling angle and printing hatch—affect the tensile strength of the specimens. Here, printing hatch is defined as the center-to-center distance between adjacent printing paths, while filling angle refers to the acute angle between the deposition paths and the loading direction (as illustrated in Figure **1**). The remaining process parameters were held constant, such as: nozzle temperature with 230°C, bed temperature with 55°C, printing speed with 270 mm/s, layer thickness with 0.2 mm, linear filling pattern, and 100% infill density.

Table 1: Printing Parameters for PLA-CF

Parameter	Value
Nozzle diameter (mm)	0.4
Nozzle temperature (°C)	230
Bed temperature (°C)	55
Printing speed (mm/s)	270
Layer thickness (mm)	0.2
Infill density (%)	100
Infill pattern	Linear
Fiber mass fraction (wt.%)	4、7、15
Printing hatch (mm)	0.35、0.45
Filling angle (°)	0、45、90

To further explore the regulatory effect of heat treatment on the anisotropic behavior of the material, this study selected representative specimens with a fiber mass fraction of 7 wt.%, a printing hatch of 0.45 mm, and filling angles of 0° and 90° for heat treatment experiments. The specific heat treatment process parameters are listed in Table **2**.

Table 2: Annealing Parameters for PLA-CF

Equipment	Annealing temperature (°C)	Annealing time (h)
Muffle furnace	100	2、8
Vacuum drying oven	180	3

2.3. Characterization and Equipment

To ensure the reliability of experimental data, three parallel specimens were prepared for each parameter combination to minimize experimental errors. Considering the hygroscopic nature of PLA material, all filaments were pretreated using a DZF-6050 vacuum drying oven (Shaoxing Yicheng Instrument Manufacturing Co., Ltd, China) under the condition of 50°C and 12h before printing. Uniaxial tensile tests were conducted at room temperature using a CMT5105 electronic universal testing machine (Zhuhai Sansi-Taijie Electric Equipment Co., Ltd, China). The testing system was equipped with a Transcell PTSH-10t force sensor. During the experiment, the crosshead load rate was maintained at 2 mm/min with preload force of 50 N and clamping pressure of 4 MPa, and the test continued until complete specimen fracture. The tensile strength was calculated using the following equation.

$$\sigma_f = \frac{F_m}{b \times d}$$

Where σ_f denotes tensile strength, F_m denotes maximum force during experiment, b denotes the width of specimen and d denotes the thickness of specimen. To ensure the reliability and repeatability of the experimental results, three samples were printed for each parameter combination, and their tensile properties were tested and the mean and standard deviation were calculated.

Specimens with a printing hatch of 0.45 mm, filling angles of 0° and 90°, and a fiber mass fraction of 7% were selected for the anisotropic optimization experiment of heat treatment. Before experiments, to determine the heat treatment temperature, the DSC method was used to measure the glass transition temperature, crystallization temperature, and melting temperature of PLA-CF specimens. DSC testing was performed using the TA-DSC2500 device. The specimens mass of DSC testing was 10 mg. They were heated to 250°C at a rate of 10°C/min under a nitrogen atmosphere, and then cooled to room temperature at a rate of 10°C/min.

Heat treatment experiments were conducted using a muffle furnace (annealing at 100°C) and a DZF6050 vacuum drying oven with a heating rate of 10°C/min. It should be mentioned that the vacuum drying oven heats the sample using hot air blowing, therefore the set temperature and the actual temperature obtained by the sample will differ. In this study, when it was set to 180°C, the actual annealing temperature of the sample maintained at 150°C, which was ensured by external heating coupler. After heating from room temperature to the annealing temperature, the specimens were held for the annealing time, and then the furnace and the vacuum drying oven were turned on for cooling. When using the vacuum drying oven for heat treatment, a vacuum of -0.1 MPa was maintained.

The microstructure of the fracture surfaces of the specimens was observed using a COXEM EM-30 scanning electron microscope at an accelerating voltage of 15 kV. A portion of the fractured specimen was cut 5 mm from the fracture surface using a wire saw, and the cut specimen was adhered to the sample stage with conductive adhesive. To improve imaging results, all specimens underwent 300 seconds of gold spraying using a Mini Coater gold coater from Shenzhen Sup Instrument Co., Ltd.

3. RESULTS AND DISCUSSION

3.1. Tensile Property Analysis

The results of the uniaxial tensile tests of directly formed 3D printed PLA-CF are shown in Table **3** and Figure **2**. It can be seen that with different printing parameters, the minimum σ_f is 19.22 MPa, and the maximum is 51.35 MPa, indicating that the printing parameters have a significant impact on the tensile strength of the specimens. To better understand the effect of different parameters on the tensile strength of PLA-CF specimens, some subfigures are used to present these results. The effects of fiber mass fraction, printing hatch, and filling angle on the tensile strength of the specimens are discussed in three separate subsections.

Table 3: Tensile Test Results of the Specimens and Process Parameter Ranges

Specimens	Filling angle = 90°	Filling angle = 45°	Filling angle = 0°
	σ_f (MPa)	σ_f (MPa)	σ_f (MPa)
Fiber mass fraction =4 Printing hatch =0.35	31.60±0.86	35.66±0.42	51.35±0.38
Fiber mass fraction =4 Printing hatch =0.45	29.50±1.24	34.44±0.47	50.55±2.42
Fiber mass fraction =7 Printing hatch 0.35	26.69±0.93	30.34±0.14	46.12±0.52
Fiber mass fraction =7 Printing hatch 0.45	19.22±0.54	23.37±0.30	44.75±0.69
Fiber mass fraction =15 Printing hatch= 0.35	30.42±1.48	33.42±0.43	41.44±0.81
Fiber mass fraction =15 Printing hatch =0.45	29.18±1.04	32.46±0.68	45.27±0.55

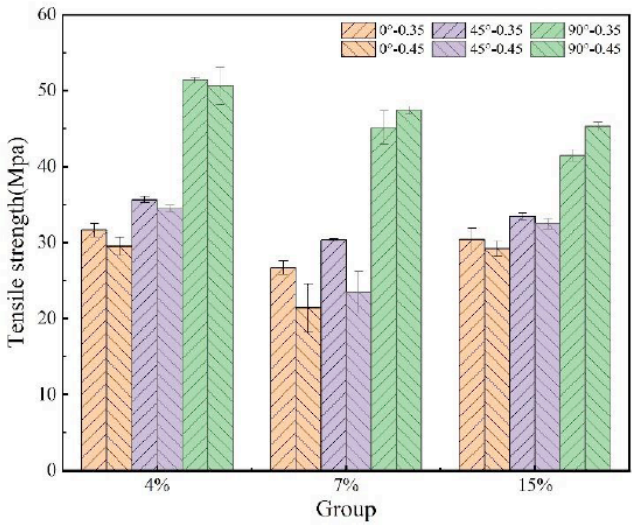


Figure 2: Tensile stress of PLA-CF specimens.

3.1.1. Effects of Filling Angle on Tensile Strength

The filling angle is the acute angle formed between the direction of material deposition by the nozzle during 3D printing and the direction of force application in tensile testing. As the filling angle decreases, the tensile strength of PLA-CF specimens with three different fiber mass fractions gradually increases, as indicated by the black arrows in the Figure **3**. When the filling angle is 0°, the tensile strength of PLA-CF specimens with three fiber mass fraction and printing hatch of 0.35 mm and 0.45 mm reaches the maximum values, which are 51.35 MPa, 50.55 MPa, 46.12 MPa, 44.75 MPa, 41.44 MPa, and 45.27 MPa, respectively.

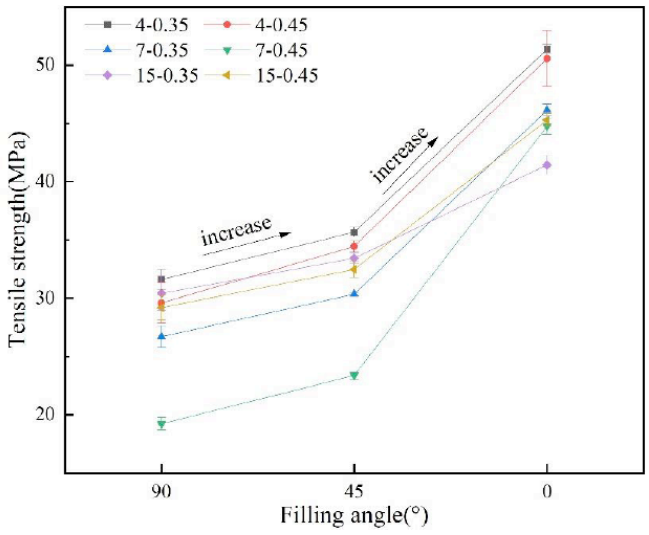


Figure 3: The effect of filling angle on the tensile strength of PLA-CF specimens.

When the printing hatch is 0.35 mm and the fiber mass fraction is 4%, the tensile strength of the specimens increases by 12.85% as the filling angle changes from 90° to 45°, and when the filling angle is 0°, the tensile strength increases by 62.5% compared to 90°. This is because FDM-printed specimens are affected by the process, showing strong anisotropic behavior. During material extrusion, the molecular chains of the matrix form locally ordered structures along the forming direction, providing self-reinforcement. Therefore, when the filling angle is 0°, the reinforcement effect is most pronounced, and the tensile strength is highest. When the filling angle is 90°, the self-reinforcement effect is not obvious, and the tensile strength mainly relies on interlayer bonding to resist tensile load, resulting in the lowest tensile strength. In addition, the orientation of the carbon fibers is also influenced by the flow direction during matrix extrusion, causing most of the fibers to align along the forming direction. When the filling angle is 0°, the fibers can transfer part of the load through interface bonding stress between the fibers and the matrix, which also enhances the tensile strength. However, the fibers basically do not bear axial load, so the tensile strength is lowest at 90°.

3.1.2. Effects of Printing Hatch on Tensile Strength

In the FDM printing process, the printing hatch refers to the distance between the centerlines of adjacent extruded paths in the same plane. It can be observed in Figure **4** that when the filling angles are 90° and 45°, the tensile strength of specimens with a printing hatch of 0.35 mm is higher than that of specimens with a printing hatch of 0.45 mm. However, when the filling angle is 0°, the printing hatch has little effect on the tensile strength of the specimen. Specifically, when the fiber mass fraction is 15 wt.%, reducing the printing hatch actually increases the tensile strength of the specimen, as indicated by the red arrow in the figure. This is because as the printing hatch increases, the distance between two adjacent extruded paths becomes larger. Under the conditions of constant nozzle diameter and extrusion flow, the overlapping area between the two matrix paths decreases, weakening the molecular diffusion and mechanical bonding between paths. For 90° specimens, the tensile load acts on the bonding surface between the matrices, and increasing the printing hatch reduces the bonding area, which becomes a weak point during the tensile process, leading to a decrease in tensile strength. For 45° specimens, reducing the bonding area similarly decreases the load-bearing capacity, and under the action of tensile stress and shear stress, the interface fails prematurely, reducing the tensile strength. For 0° specimens, the tensile load is parallel to the print path, and the stress is continuously transmitted within the matrix, not relying on the strength of the bonding interface, so the effect is minimal.

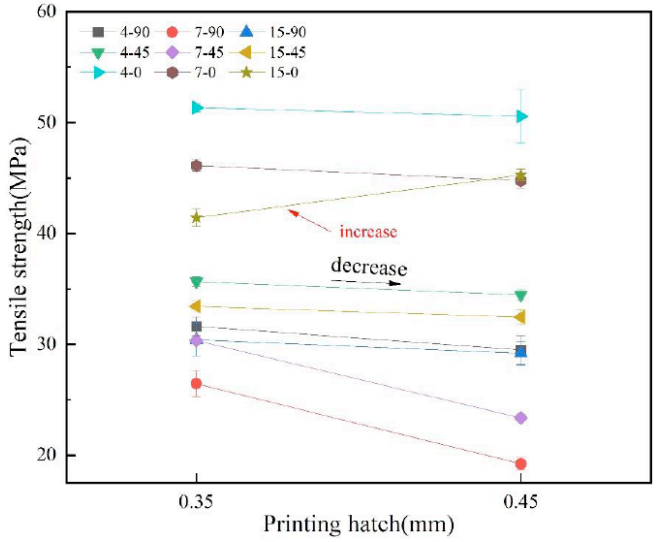


Figure 4: The effect of printing hatch on the tensile strength of PLA-CF specimens.

3.1.3. Effects of Fiber Mass Fraction on Tensile Strength

As shown in Figure **5**, the effect of carbon fiber mass fraction on tensile strength varies depending on the filling angle. When the printing hatch is 0.35 mm and the filling angle is 0°, the tensile strength of the specimen decreases as the fiber mass fraction increases. When the fiber mass fraction is 4%, the tensile strength of the specimen is the highest, at 51.35 MPa, whereas when the fiber mass fraction increases to 15%, the tensile strength decreases to 41.44 MPa, with a drop of 19.3%.

When the printing hatch is 0.35 mm and the filling angles are 90° and 45°, the tensile strength of the specimen first decreases and then increases as the fiber mass fraction increases, with the lowest strength observed at 7% fiber mass fraction, being 26.69 MPa and 30.34 MPa, respectively. When the fiber mass fraction is reduced to 4%, the tensile strength increases to 31.60 MPa and 35.66 MPa, an increase of 18.4% and 17.53%; when the fiber mass fraction increases to 15%, the tensile strength rises to 30.42 MPa and 33.42 MPa, an increase of 13.98% and 10.15%.

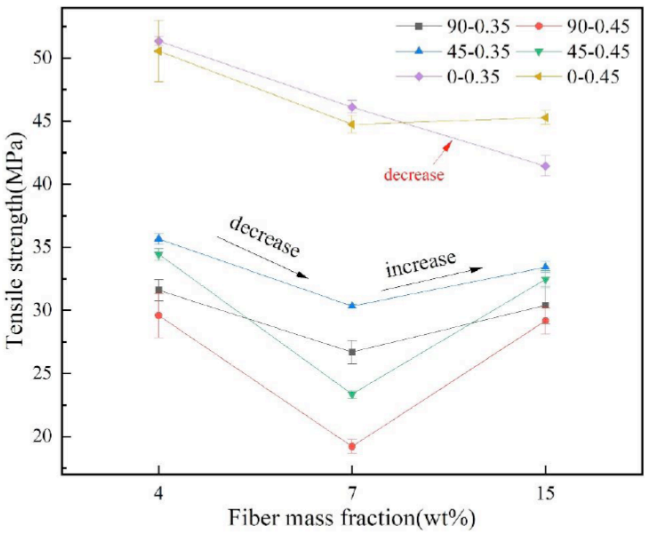


Figure 5: The effect of fiber mass fraction on the tensile strength of PLA-CF specimens.

It is worth noting that when the printing hatch is 0.45 mm and the carbon fiber mass fraction is 4% and 7%, the tensile fracture of the specimens appears as a stepped shape as shown in Figure **6**. This is considered to be due to the overly large printing hatch, resulting in a low sample building rate and small bonding area between each layer of the matrix, making it unable to withstand the shear load imposed by the tensile test, leading to failure. When the fiber mass fraction is 15%, the tensile strength of the specimens decreases, and the section perpendicular to the load is damaged first, disrupting the continuity of the matrix and interrupting the stress transfer path. At this point,

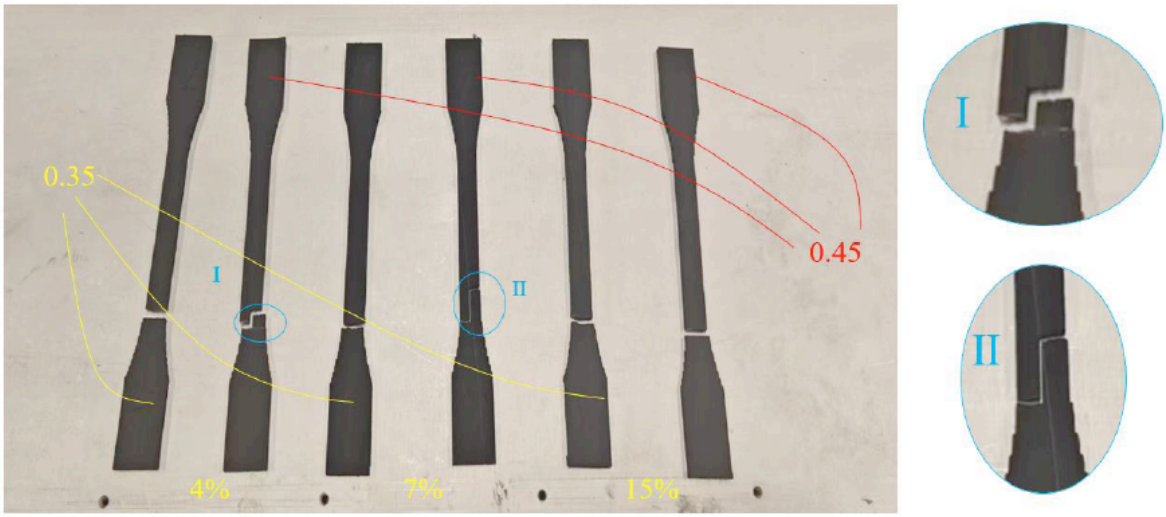


Figure 6: Fractured specimens of PLA-CF.3.2 Fracture analysis.

the load borne by the bonding surface has not reached the shear limit, so the bonding between the resin layers remains relatively intact without fracture, resulting in a straight fracture surface.

3.2. Fracture Analysis

Figure **7** shows the SEM morphology of the fracture surface of PLA-CF composite tensile specimens with filling angle of 0° and fiber mass fraction of 4%. By comparing the microstructural differences under different printing hatch conditions, one can gain a deeper understanding of the mechanism by which printing hatch affect material interlayer bonding behavior. In the specimen with a printing hatch of 0.35 mm (Figure **7**(**a**)), the fracture surface exhibits a regular rectangular fracture morphology, with a complete bonding interface formed between adjacent melt tracks, only a few tiny gaps present, small interlayer porosity, and carbon fibers uniformly dispersed within the matrix. This structural feature is due to the smaller printing hatch increasing the overlap ratio of the melt tracks, enlarging the contact area between PLA tracks, while also expanding the heat-affected zone, which promotes the diffusion of PLA molecular chains and the uniform dispersion of fibers. In contrast, the specimen with a 0.45 mm printing hatch (Figure **7**(**b**)) shows that due to the reduced heat-affected zone, the diffusion of PLA molecular chains is limited, leading to only partial interlayer bonding, a larger interlayer porosity, and obvious fiber agglomeration.

Figure **8** shows the SEM morphology of the fracture surfaces of tensile specimens of PLA-CF composites with different carbon fiber mass fraction, printed with a printing hatch of 0.35 mm and a filling angle of 90°. When the fiber mass fraction is 4% (Figure **8**(**a**) and Figure **8**(**b**)), a multi-scale composite failure mode is observed: fiber pull-out caused by debonding at the fiber-matrix interface indicates low interfacial bonding strength; the weak bonding between fibers and matrix results in fibers not providing reinforcement but instead becoming stress concentration points in the continuous matrix, weakening the matrix's load-bearing capacity; after specimen fracture, fibers pull out from the matrix, causing fiber debonding. At the same time, the weakened matrix forms crack initiation points at the fiber-matrix interface, where cracks extend into the matrix and interact with the stress fields of adjacent fibers, ultimately forming a brittle macroscopic fracture surface; some fibers are level with the surrounding matrix, indicating high interfacial bonding strength and effective load bearing by the fibers; the matrix exhibits a mixed characteristic of ductile and brittle fracture simultaneously. When the fiber mass fraction increases to 7% (Figure **8**(**c**) and Figure **8**(**d**)), the material failure mechanism significantly changes: the higher fiber content results in more fibers aligned along the printing direction; since the filling angle is 90°, these oriented fibers are perpendicular to the tensile load direction and cannot effectively carry the load, instead reducing fiber spacing and creating numerous stress concentration points in the matrix, ultimately shifting the failure mode to be dominated by brittle matrix fracture and reducing the tensile strength of the specimen. As the fiber mass fraction increases to 15% (Figure **8**(**e**) and Figure **8**(**f**)), some fibers begin to align along the load direction, showing a large number of fiber fracture features, indicating that the fibers bear the corresponding load. In addition, the fibers oriented along the load direction effectively share the principal stress, reducing the equivalent stress experienced by the matrix, allowing the local plastic deformation capacity to be released, showing characteristics of ductile fracture.

Figure **9** shows the SEM morphological characteristics of the fracture surfaces of PLA-CF

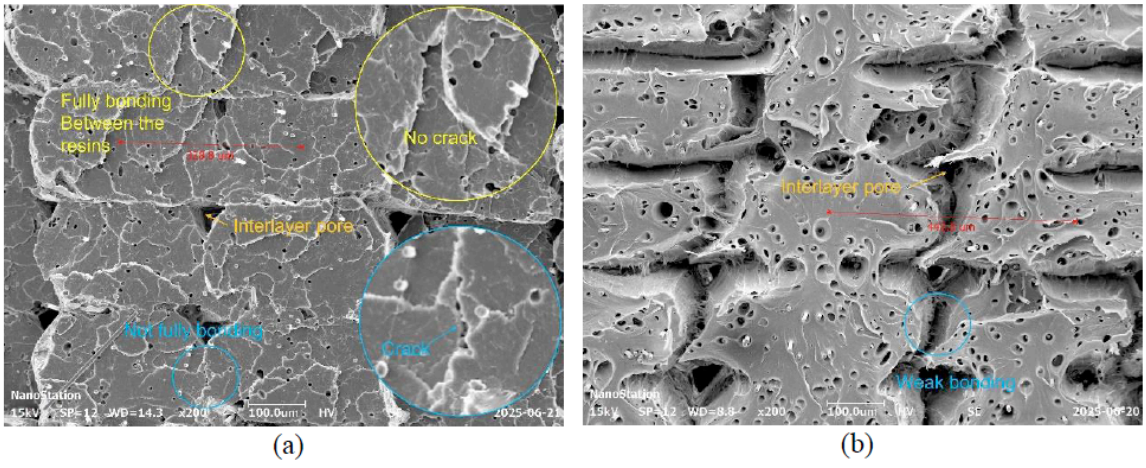


Figure 7: Fracture of PLA-CF specimens with printing hatch of (**a**) 0.35 mm and (**b**) 0.45 mm in filling angle of 0° and fiber mass fraction of 4%.

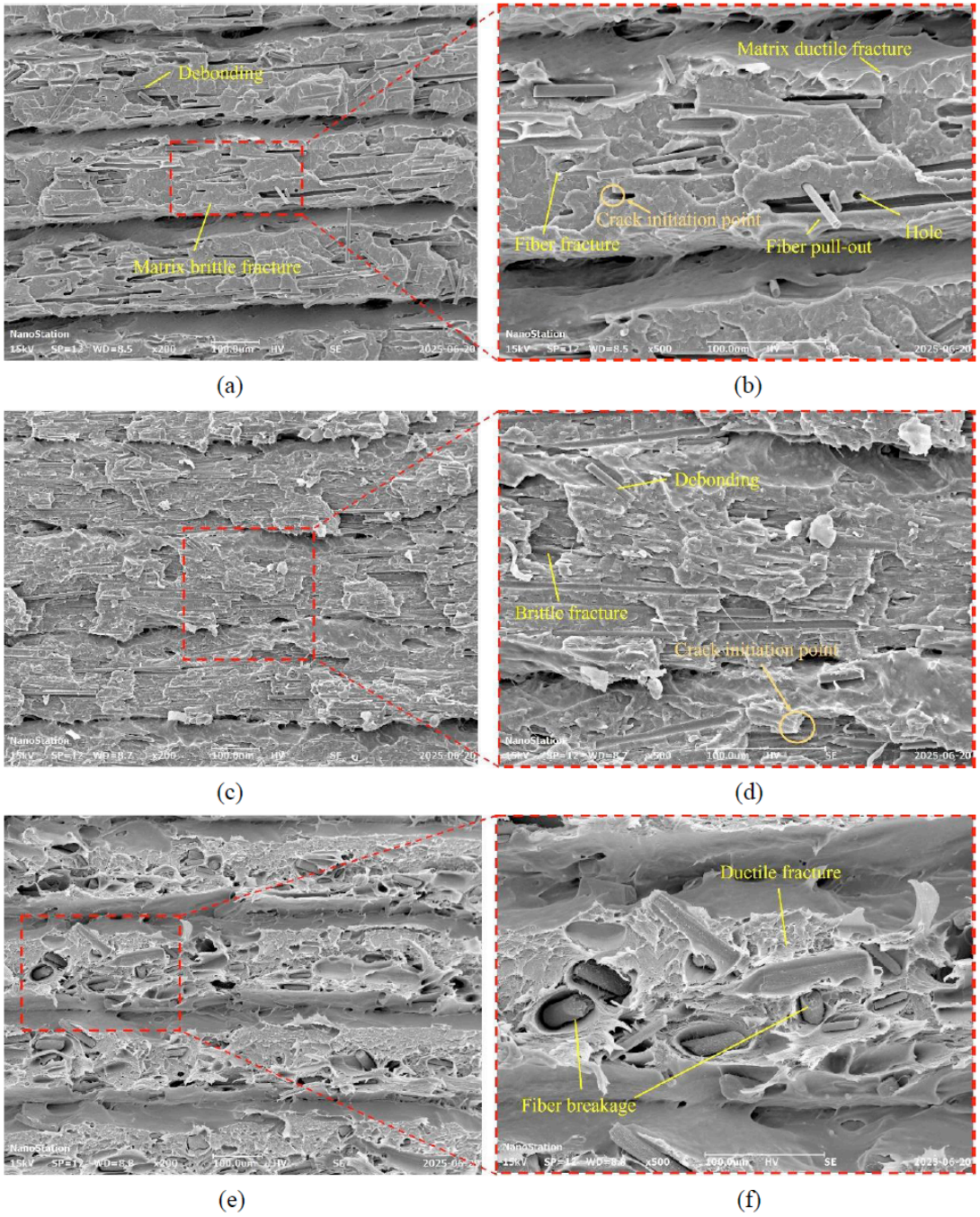


Figure 8: Fracture of PLA-CF specimens with fiber mass fraction of (**a**)(**b**) 4%, (**c**)(**d**) 7% and (**e**)(**f**) 15% in filling angle of 90° and printing hatch of 0.35 mm.

composite tensile specimens with different fiber mass fractions, printed with a printing hatch of 0.35 mm and a filling angle of 0°. In specimens with 4% fiber mass fraction (Figure **9**(**a**) and Figure **9**(**b**)), the matrix remains structurally intact, and the main failure mode is brittle fracture of the matrix accompanied by fiber pull-out and breakage. When the mass fraction increases to 7% (Figure **9**(**c**) and Figure **9**(**d**)), significant matrix cracking and numerous fiber pull-out features are observed, and the proportion of interfacial defects significantly increases. In particular, Figure **9**(**d**) shows holes and tearing on the sides of the fractured matrix. The former are the voids left in the matrix by poorly bonded fibers being pulled out, while the latter result from interfacial failure between the fibers and the matrix under shear load. When the fiber mass fraction further increases to 15% (Figure **9**(**e**) and Figure **9**(**f**)), the proportion of fibers oriented perpendicular to the loading direction increases. These fibers not only fail to bear the load but also weaken the strength of the matrix. Additionally, large-scale fiber agglomerates are formed, around which micro-scale voids exist. The load on the matrix cannot be effectively transferred to the fibers, reducing the effective load-bearing interface of the PLA matrix and significantly weakening the tensile performance of the specimens. Therefore, as the carbon fiber mass fraction increases, the tensile strength of the specimens gradually decreases.

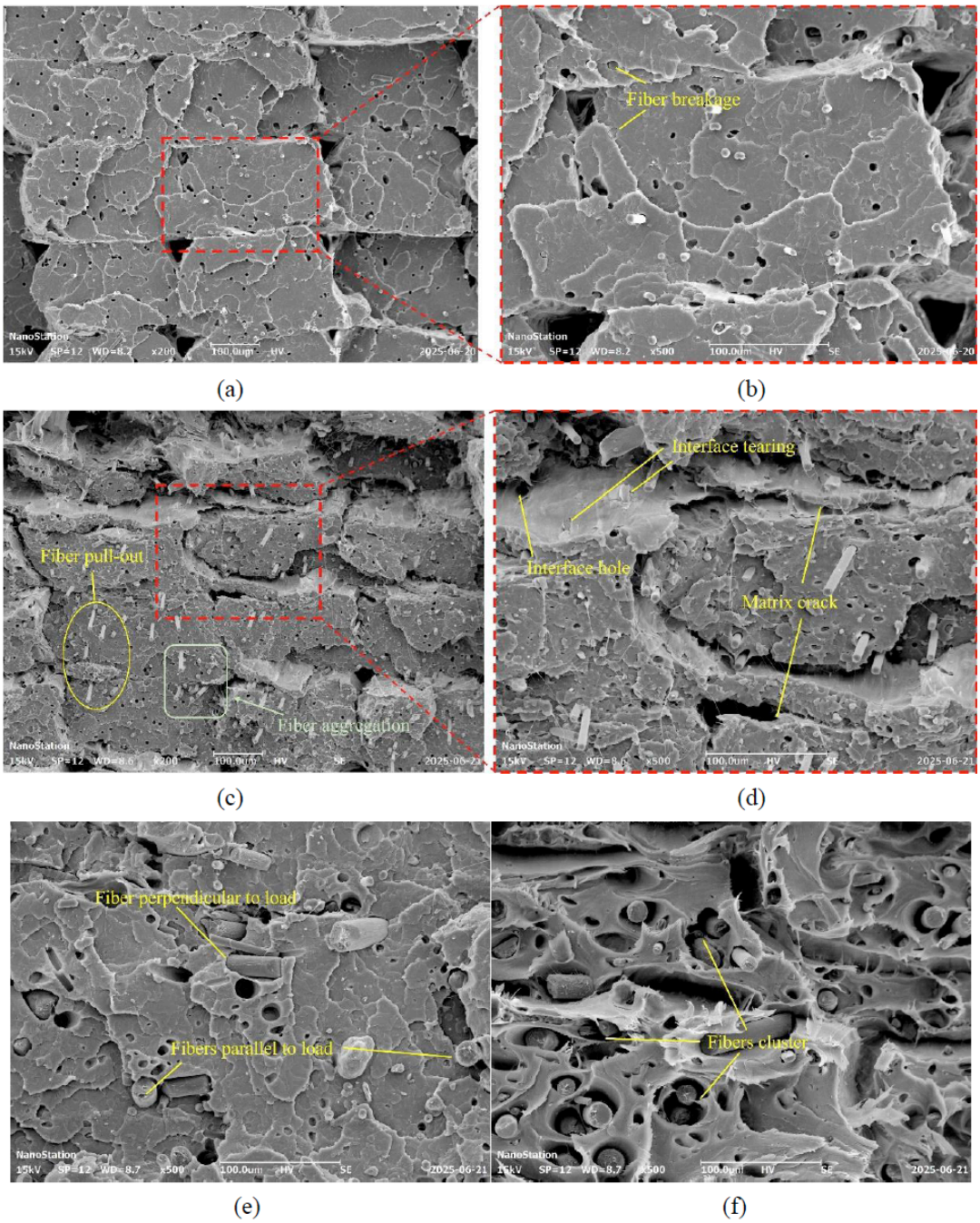


Figure 9: Fracture of PLA-CF specimens with fiber mass fraction of (**a**)(**b**) 4%, (**c**)(**d**) 7% and (**e**)(**f**) 15% in filling angle of 0° and printing hatch of 0.35 mm.

Figure **10** shows the SEM morphology characteristics of the fracture surfaces of PLA-CF composite tensile specimens with different carbon fiber mass fraction, printed with a printing hatch of 0.35 mm and a filling angle of 45°. When the fiber mass fraction is 4% (Figure **10**(**a**) and Figure **10**(**b**)), the fracture exhibits a mixed mode of 0° and 90° fracture. Among them, the 90° fracture feature is manifested as matrix delamination, that is, the matrix is damaged in the printing plane perpendicular to the printing direction, while the 0° fracture feature includes fiber pull-out, fiber breakage, and brittle fracture of the matrix in the printing plane along the printing direction. This mixed fracture mode results in the tensile strength of the 45° specimens being between that of the 0° and 90° specimens. When the fiber mass fraction is 7% (Figure **10**(**c**)), the specimens maintain a similar fracture mode, but interlayer fusion defects lead to increased porosity, generating stress concentrations that reduce strength. When the fiber mass fraction increases to 15% (Figure **10**(**d**)), the fracture mechanism changes significantly: in addition to fiber breakage and fiber pull-out, there are also numerous plastic deformation features such as dimples. These plastic deformations gradually absorb the energy of tensile failure through energy dissipation mechanisms, thereby improving the strength of the specimens.

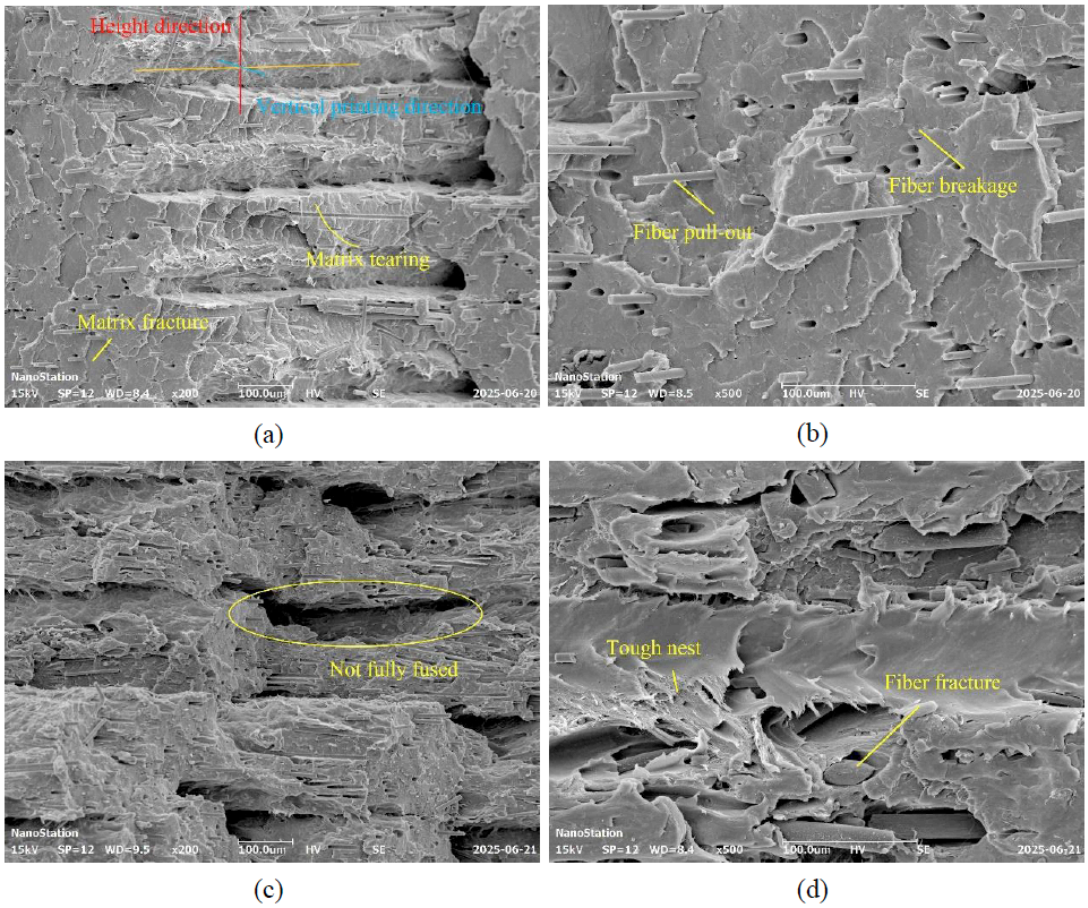


Figure 10: Fracture of PLA-CF specimens with fiber mass fraction of (**a**)(**b**) 4%, (**c**) 7% and (**d**) 15% in filling angle of 45° and printing hatch of 0.35 mm.

3.3. Effect of Heat Treatment

3.3.1. Result of DSC Experiment

Figure **11** shows the DSC curves of unprinted filament and printed specimens. The specimens were heated from room temperature to 250°C at a rate of 10°C/min under nitrogen and then cooled back to room temperature. From the figure, the glass transition temperature (T_g) of the specimen is 65°C, the cold crystallization temperature (T_c) is 110°C, and the melting temperature (T_m) is 148°C. It is noteworthy that an additional cold-crystallization peak appears at approximately 75 °C in the printed specimens—a feature absents in the unprinted filament. This discrepancy can be attributed to the thermal history imposed by the FDM process. During extrusion and subsequent cooling, the PLA molecular chains undergo flow-induced orientation and develop a degree of structural order. However, due to rapid cooling and limited time for molecular rearrangement, full crystallization is not achieved. Consequently, some molecular chains remain in a metastable (partially ordered) state, capable of further crystallization upon reheating. The additional peak at ~75 °C indicates the presence of molecular chains with higher mobility and a relatively lower energy barrier for crystallization, whereas the primary cold-crystallization peak at ~110 °C corresponds to the crystallization of the remaining amorphous PLA chains at a higher temperature. These thermal transition characteristics suggest that the printed PLA-CF composites retain a significant potential for thermally induced structural rearrangement, providing a theoretical basis for tailoring their interlayer bonding and mechanical properties through post-process heat treatment.

The DSC results also offer a thermal explanation for the observed changes in tensile strength and mechanical anisotropy following annealing. At 100 °C, the PLA matrix is heated above its glass transition temperature, which enhances chain segment mobility and facilitates molecular interdiffusion at interfaces that were not fully bonded. Meanwhile, this temperature remains below both the primary cold-crystallization temperature and the melting point. This increased molecular mobility, combined with the potential for further crystallization—as evidenced by the low-temperature exothermic peak—promotes interlayer fusion and alters the stiffness and toughness of the matrix. Furthermore, during vacuum annealing, the actual temperature of the specimens reaches approximately 150 °C, a value near or slightly above the experimentally determined melting point of 148 °C.

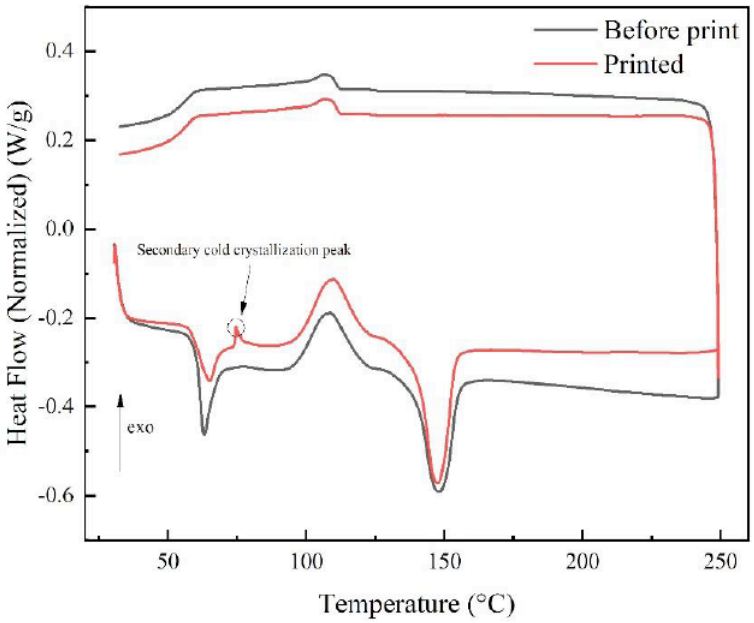


Figure 11: DSC curves of unprinted filament and printed specimen.

Under these conditions, the PLA matrix may undergo significant melting or remelting, which facilitates reconsolidation between adjacent deposited beads. Meanwhile, the vacuum environment helps expel internal gases and reduce porosity. These findings will provide a basis for analyzing the subsequent evolution of tensile properties, interlayer bonding characteristics, and mechanical anisotropy under various heat treatment conditions.

3.3.2. Analysis of Mechanical Properties and Microstructure

The tensile strength results are shown in Figure **12**, where the UT refers to specimens that were not heat-treated, 100-2 and 100-8 refers to specimens kept in the muffle furnace at 100°C for 2 hours and at 100°C for 8 hours, and v180-3 refers to specimens kept in the vacuum drying oven at 180°C for 3 hours.

The results are shown in Figure **12**. Heat treatment at 100°C for 2 hours in the furnace increased the tensile strength of the filling angle of 90° printed specimens from 19.22 MPa to 31.6 MPa, a significant improvement of 64.4%. However, the tensile strength of the filling angle of 0° printed specimens decreased from 44.75 MPa to 42.1 MPa, a reduction of 6.3%. As the holding time increased to 8 hours, the tensile strength of specimens with filling angles of 0° and 90°

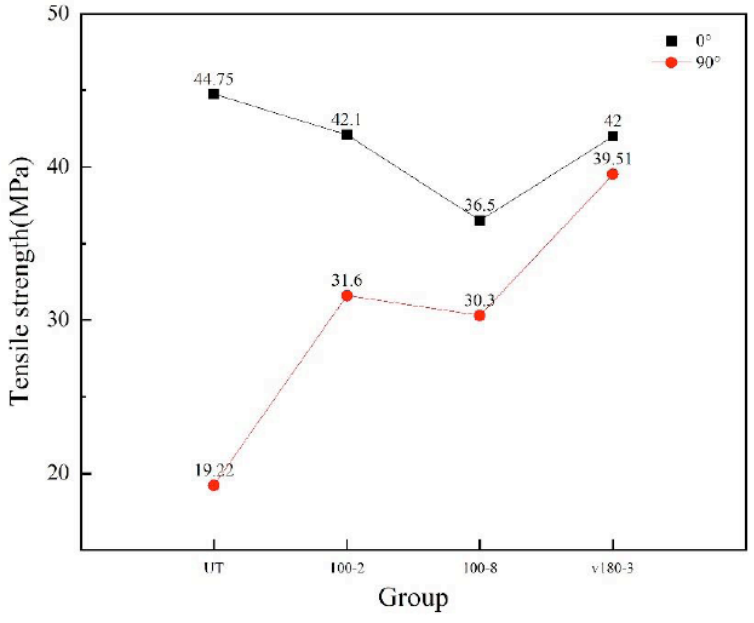


Figure 12: The effect of annealing parameters on tensile strength of PLA-CF specimens.

decreased to varying degrees compared with the 2-hour holding group, but the tensile strength of the 90° filling angle specimens was still 57.6% higher than that of the UT group. This can be explained by Figure **13**: after heat treatment, the interlayer voids between each layer of the 3D-printed resin matrix were completely eliminated, indicating that the resin between and within layers had fully remelted together, thus enhancing the interlayer bonding strength, which significantly improved the tensile strength of the 90° specimens. However, heat treatment also increased the crystallinity of the PLA matrix. With prolonged holding time, more PLA molecules completed crystallization, reducing the toughness of the specimens, so the fracture characteristics of the 0° specimen matrix changed from ductile to brittle, resulting in a decrease in tensile strength. After heat treatment in a vacuum drying oven, the tensile strength of the 90° specimens further increased to 39.51 MPa, an improvement of 105.6% compared with untreated specimens, and only 2.5 MPa lower than that of the 0° specimens. As shown in Figure **14**(**a**) and Figure **14**(**b**), specimens treated in the vacuum drying oven not only allowed the resin layers to recombine but also the low pressure promoted the escape of internal bubbles in the matrix, reducing internal defects in the specimens; thus, the 90° specimens had the highest tensile strength among all specimens. Figure **14**(**c**) and Figure **14**(**d**) show that although the 0° specimens also experienced the ductile-to-brittle transition due to the increased PLA crystallinity, forming large areas of brittle fracture patterns, the carbon fibers were mainly oriented along the loading direction, and the ability of the fibers to bear axial loads still allowed them to maintain mechanical properties better than the 90° specimens.

4. CONCLUSIONS

This study systematically investigated the tensile properties and anisotropy of FDM-printed short carbon fiber-reinforced PLA composites, focusing on the effects of fiber mass fraction, filling angle, printing hatch, and post heat treatment. The main conclusions are as follows:

1) The tensile properties of FDM-printed PLA-CF composites are significantly influenced by the infill angle, print spacing, and carbon fiber mass fraction. The material exhibits its highest tensile strength—51.35 MPa—when the infill angle is 0°, the print spacing is 0.35 mm, and the carbon fiber mass fraction is 4 wt.%. For infill angles of 45° and 90°, reducing the print spacing enhances tensile strength; the impact of fiber content, meanwhile, depends on the infill angle—a result of the complex interplay between factors such as fiber orientation, interfacial bonding, and the formation of defects.

2) Analysis of tensile fracture surfaces reveals that the material's fracture behavior is primarily governed by fiber orientation, fiber-matrix interfacial bonding, and interlayer defects. A

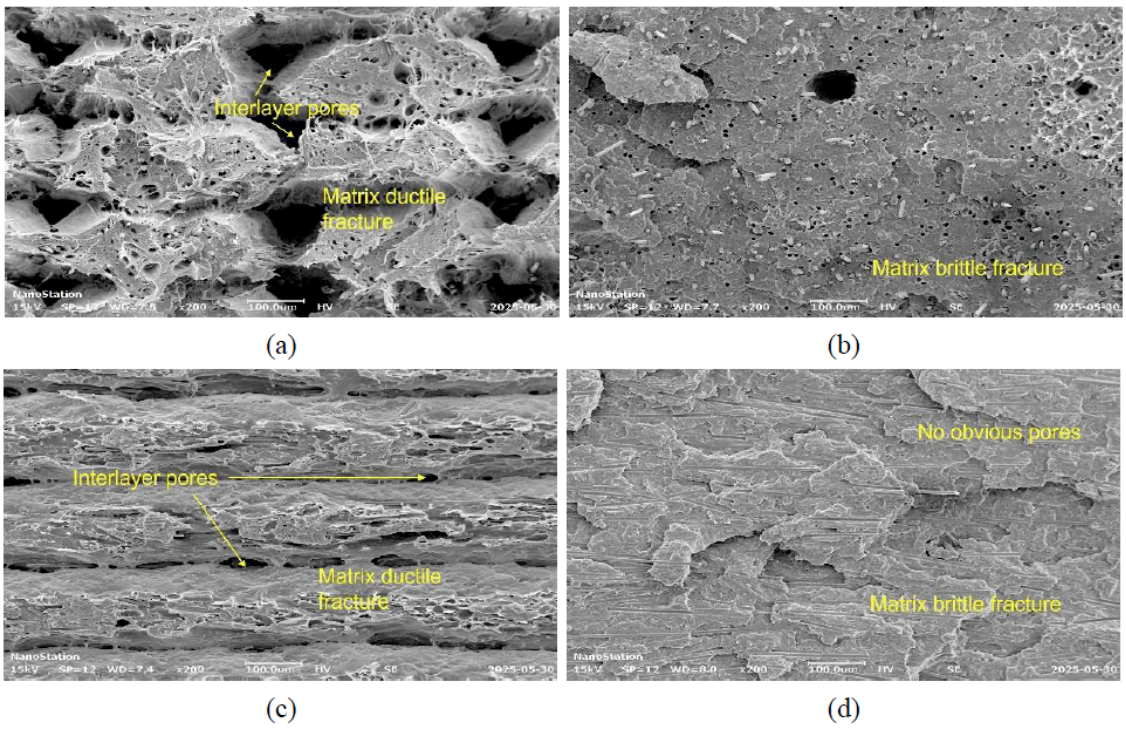


Figure 13: Fracture of untreated PLA-CF specimens with filling angle of (**a**) 0° and (**c**) 90°, and treated by 100-8 with filling angle of (**b**) 0° and (**d**) 90°.

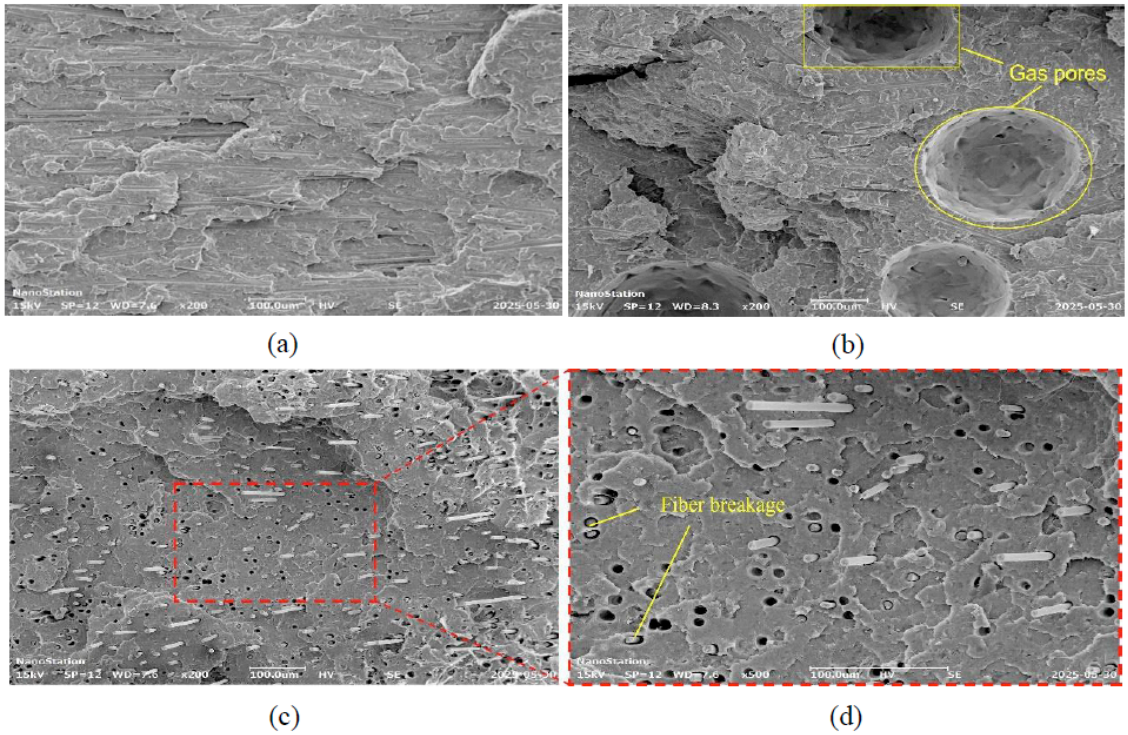


Figure 14: Fracture of PLA-CF specimens treated by v180-3 with filling angle of (**a**) 90° and (**c**)(**d**) 0°, and (**b**) treated by 100-8 with filling angle of 90°.

smaller print spacing promotes more continuous bonding between print paths and reduces noticeable interlayer gaps. Conversely, at high fiber contents, phenomena such as fiber agglomeration and fiber pull-out become more pronounced.

3) Heat treatment significantly enhances the tensile strength of specimens printed with a 90° infill angle while reducing their mechanical anisotropy. Annealing at 100°C for 2 hours increases the tensile strength from 19.22 MPa to 31.60 MPa. Furthermore, a 3-hour vacuum heat treatment at approximately 150°C (actual specimen temperature) boosts the tensile strength to 39.51 MPa—a 105.6% improvement over the untreated specimens. Under these conditions, the strength disparity between the 0° and 90° specimens narrows to 2.5 MPa, demonstrating the effectiveness of appropriate post-processing in enhancing interlayer integrity and improving mechanical consistency.

This work provides an effective strategy for optimizing printing parameters and post-treatment to achieve high-performance and low anisotropy PLA-CF components for FDM engineering applications. It also should be mentioned that the biodegradability of the composites was not studied, which will be conducted in future work.

DECLARATION OF INTERESTS

The authors declare that they have no known competing financial interests or personal relationships that could have appeared to influence the work reported in this paper.

ACKNOWLEDGEMENTS

This work was supported by China Postdoctoral Science Foundation (Grant No. 2025M774302), and Guangdong Basic and Applied Basic Research Foundation (Grant No. 2024A1515012049).

AUTHOR'S CONTRIBUTION STATEMENT

Yuchao Bai: Supervision, Investigation, Writing - Original Draft, Funding acquisition. ***Yihan Xiao:*** Conceptualization, Data curation. ***Yilin Wang:*** Visualization, Formal analysis. ***Yilin Liang:*** Methodology, Investigation. ***Yu Yan:*** Methodology, Validation. ***Cuiling Zhao:*** Funding acquisition, Writing-Reviewing and Editing

REFERENCE

[1] Yuan S, Li S, Zhu J, *et al*. Additive manufacturing of polymeric composites from material processing to structural design. Composites Part B: Engineering 2021; 219. https://doi.org/10.1016/j.compositesb.2021.108903

[2] Goh GD, Wong KK, Tan N, *et al*. Large-format additive manufacturing of polymers: a review of fabrication processes, materials, and design. Virtual and Physical Prototyping 2024; 19(1). https://doi.org/10.1080/17452759.2024.2336160

[3] Zhang T, Lin X, Qin Y, *et al*. Multiphysics Modeling of Heat Transfer and Melt Pool Thermo-Fluid Dynamics in Laser-Based Powder Bed Fusion of Metals. Materials (Basel) 2025; 18(13). https://doi.org/10.3390/ma18133183

[4] Bourell DL. Perspectives on Additive Manufacturing. Annual Review of Materials Research 2016; 46(1): 1-18. https://doi.org/10.1146/annurev-matsci-070115-031606

[5] Abderrafai Y, Diouf-Lewis A, Sosa-Rey F, *et al*. Additive manufacturing and characterization of high temperature thermoplastic blends for potential aerospace applications. Composites Science and Technology 2023; 231. https://doi.org/10.1016/j.compscitech.2022.109839

[6] Chrz K, Bruthans J, Ptacnik J. Clinical Application of FDM 3D Printing in Surgery and Traumatology: A Systematic Review. Ann Biomed Eng 2026. https://doi.org/10.1007/s10439-026-04021-z

[7] Bere P, Neamtu C, Udroiu R. Novel Method for the Manufacture of Complex CFRP Parts Using FDM-based Molds. Polymers (Basel) 2020; 12(10). https://doi.org/10.3390/polym12102220

[8] Omer MAE, Shaban IA, Mourad A-H, *et al*. Advances in interlayer bonding in fused deposition modelling: a comprehensive review. Virtual and Physical Prototyping 2025; 20(1). https://doi.org/10.1080/17452759.2025.2522951

[9] Zohdi N, Yang RC. Material Anisotropy in Additively Manufactured Polymers and Polymer Composites: A Review. Polymers (Basel) 2021; 13(19). https://doi.org/10.3390/polym13193368

[10] Madhavan Nampoothiri K, Nair NR, John RP. An overview of the recent developments in polylactide (PLA) research. Bioresour Technol 2010; 101(22): 8493-501. https://doi.org/10.1016/j.biortech.2010.05.092

[11] Arrigo R, Frache A. FDM Printability of PLA Based-Materials: The Key Role of the Rheological Behavior. Polymers (Basel) 2022; 14(9). https://doi.org/10.3390/polym14091754

[12] Changhui L, Hao L, Chunlong Y, *et al*. Balanced Optimization of Dimensional Accuracy and Printing Efficiency in FDM Based on Data-Driven Modeling. Additive Manufacturing Frontiers 2025; 4(2). https://doi.org/10.1016/j.amf.2025.200220

[13] Sukumaar VN, Rangappa SM, Liu Y, *et al*. A comprehensive review on the influence of fused deposition modelling process parameters upon thermoplastic composite materials. Advanced Industrial and Engineering Polymer Research 2026; 9(2): 281-303. https://doi.org/10.1016/j.aiepr.2025.11.006

[14] Layeb N, Oldal I, Zsidai L. Flexural strength evolution of 3D printed PLA-CF structures: optimization of FDM parameters for enhanced mechanical performance. Journal of Materials Science: Materials in Engineering 2026; 21(1). https://doi.org/10.1186/s40712-026-00424-x

[15] Plamadiala I, Croitoru C, Pop MA, *et al*. Enhancing Polylactic Acid (PLA) Performance: A Review of Additives in Fused Deposition Modelling (FDM) Filaments. Polymers (Basel) 2025; 17(2). https://doi.org/10.3390/polym17020191

[16] Haque MMM, Dhrubo SR, Pranto A-FZ, *et al*. Impact of process parameters and material selection on the mechanical performance of FDM 3D-Printed components. Hybrid Advances 2025; 10. https://doi.org/10.1016/j.hybadv.2025.100502

[17] Kamaal M, Anas M, Rastogi H, *et al*. Effect of FDM process parameters on mechanical properties of 3D-printed carbon fibre–PLA composite. Progress in Additive Manufacturing 2020; 6(1): 63-9. https://doi.org/10.1007/s40964-020-00145-3

[18] Wickramasinghe S, Do T, Tran P. FDM-Based 3D Printing of Polymer and Associated Composite: A Review on Mechanical Properties, Defects and Treatments. Polymers (Basel) 2020; 12(7). https://doi.org/10.3390/polym12071529

[19] Bhandari S, Lopez-Anido RA, Gardner DJ. Enhancing the interlayer tensile strength of 3D printed short carbon fiber reinforced PETG and PLA composites via annealing. Additive Manufacturing 2019; 30. https://doi.org/10.1016/j.addma.2019.100922

[20] Butt J, Khan MAA, Adnan M, *et al*. Performance Analysis of FFF-Printed Carbon Fiber Composites Subjected to Different Annealing Methods. Journal of Manufacturing and Materials Processing 2024; 8(6). https://doi.org/10.3390/jmmp8060252

[21] Papon EA, Haque A, Spear SK. Effects of functionalization and annealing in enhancing the interfacial bonding and mechanical properties of 3D printed fiber-reinforced composites. Materials Today Communications 2020; 25. https://doi.org/10.1016/j.mtcomm.2020.101365

https://doi.org/10.12974/2311-8717.2026.14.13

© 2026 Bai *et al.*
This is an open-access article licensed under the terms of the Creative Commons Attribution License (http://creativecommons.org/licenses/by/4.0/), which permits unrestricted use, distribution, and reproduction in any medium, provided the work is properly cited.